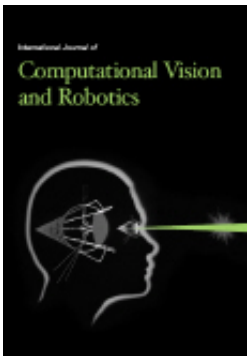

International Journal of Computational Vision and Robotics

ISSN online: 1752-914X - ISSN print: 1752-9131
https://www.inderscience.com/ijcvr

Supervised learning software model for the diagnosis of diabetic retinopathy

M. Padmapriya, S. Pasupathy

DOI: 10.1504/IJCVR.2021.10037274

Article History:

Received:	03 January 2021
Accepted:	22 February 2021
Published online:	30 November 2022

Supervised learning software model for the diagnosis of diabetic retinopathy

M. Padmapriya*

Department of Information Technology,
Saranathan College of Engineering,
Tamil Nadu, India
Email: padmapriya-it@saranathan.ac.in
*Corresponding author

S. Pasupathy

Department of Computer Science and Engineering,
Annamalai University,
Annamalai Nagar, Tamil Nadu, India
Email: pathyannamalai@gmail.com

Abstract: Diabetic retinopathy (DR) is the leading cause of eye diseases and vision loss for diabetic affected people. Due to the damage of retinal blood vessels, diabetic patients often suffer from DR. So the retinal blood vessel segmentation plays a crucial role in the diagnosis of DR. We can prevent vision loss or blindness problems if the diagnosis happens during the early stages. Early diagnosis and initial investigation would help lower the risk of vision loss by 50%. This article exploits the supervised classification approach to detect blood vessels by applying features such as grey level and invariant moments. The image pre-processing and blood vessel segmentation are the two essential steps are used in this study, along with the proposed classification framework using neural network models. Two publicly available retinal image datasets, such as DRIVE and STARE, are used to assess the proposed supervised classification framework. The suggested supervised classification methodology in this study attains the average retinal blood vessel segmentation accuracy of 93.94% in the DRIVE dataset and 95.00% in the STARE dataset.

Keywords: diabetic retinopathy; fundus imaging; grey level features; invariant moments; vessel segmentation.

Reference to this paper should be made as follows: Padmapriya, M. and Pasupathy, S. (2023) 'Supervised learning software model for the diagnosis of diabetic retinopathy', *Int. J. Computational Vision and Robotics*, Vol. 13, No. 1, pp.116–132.

Biographical notes: M. Padmapriya is a PhD candidate in the Department of Computer Science and Engineering, Annamalai University, India. She holds a ME degree in Computer Science and Engineering from Anna University, BIT Campus, Tiruchirappalli, India in the year 2012. Her research interests include software engineering and advanced soft computing.

S. Pasupathy is an Associate Professor in the Department of Computer Science and Engineering, Annamalai University, India. His area of research includes object oriented analysis and design, s/w quality assurance and testing, and data

mining. He has published more than 12 research papers in reputed international journals. He has 20 years of teaching and research experience. He has guided more than 31 MPhil/ME/MSc students and currently guiding six PhD research scholars.

1 Introduction

Diagnosing glaucoma is often a difficult job. It is often complicated, and in most cases, its prediction is doubtful. Glaucoma is the second leading cause of permanent blindness, especially in the 50 years or older group people in the world. Optic nerves' damage is the major effect of glaucoma disease, which may lead to long-lasting vision loss. But we can prevent blindness from glaucoma through early diagnosis and correct treatment. Primary open-angle glaucoma (POAG) and primary angle-closure glaucoma (PACG) are the two common forms of glaucoma (Sakthivel and Narayanan, 2015; Medha and Pradeep, 2014; Abramoff et al., 2010). The normal eye and an eye with glaucoma are shown in Figure 1.

Figure 1 (a) The normal eye and (b) an eye with glaucoma (see online version for colours)

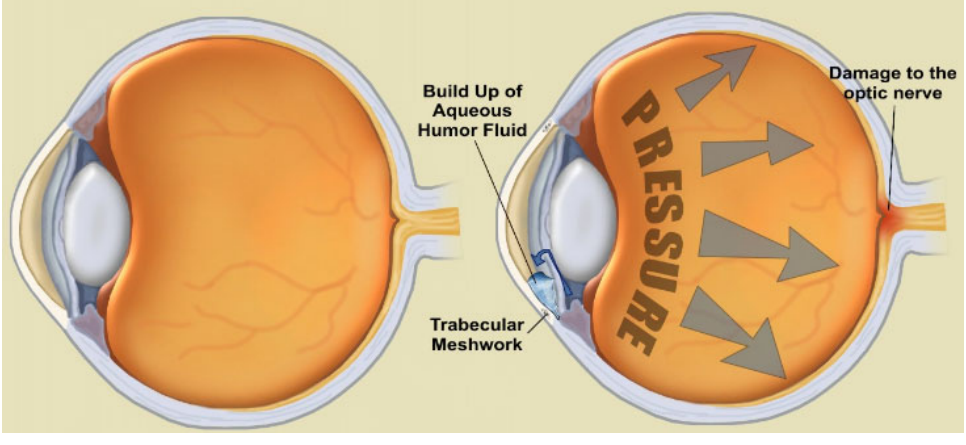

(a) (b)

It is a disease of progressive optic neuropathy with loss of retinal neurons and their axons. It is difficult or impossible to detect the early stages of optic nerve damage. In a realistic scenario, 50% of the people with glaucoma do not realise it. Most people (95%) with the elevated intraocular pressure (IOP) will never have the optic nerve damage associated with glaucoma. Most of the ocular findings in abnormal (glaucoma) people might also appear in healthy people. Hence, the early diagnosis of glaucoma becomes a more challenging task (Kanski and Bowling, 2011; Patton et al., 2006).

IOP is not only the cause of glaucoma disease. Other than IOP, age, cup-disk ratio, and central corneal thickness are the significant causes of developing POAG. Irritability, photophobia, epiphora, flickering, and low vision are the symptoms of glaucoma. The

elevated IOP, buphthalmos, Haab's striae, corneal clouding, glaucomatous cupping, and field loss are the signs of glaucoma disease (Kwon et al., 2009).

Glaucoma is a kind of disorder defined by higher IOP and the reactions of the following (Narasimhan et al., 2012):

- elevated pressure
- optic nerve atrophy
- peripheral visual field loss.

Figure 2 Retinal image datasets (see online version for colours)

Figure 3 The normal retinal image (see online version for colours)

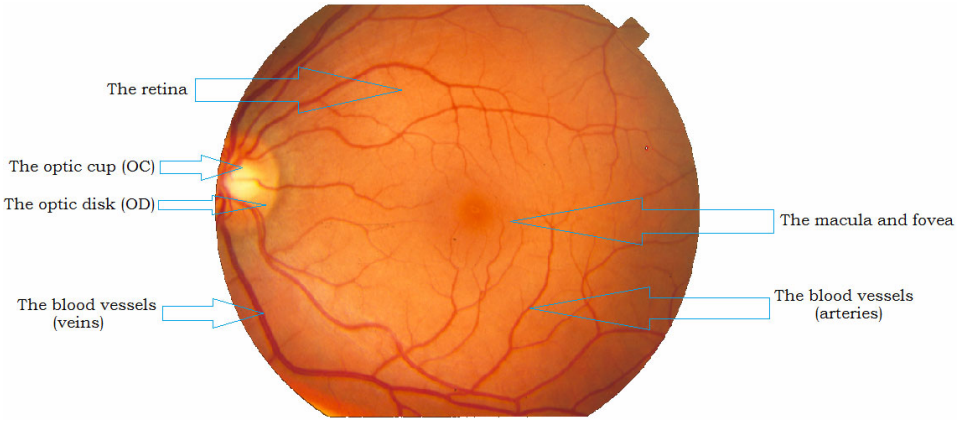

There are many publicly available retinal image datasets used to diagnosis diabetic retinopathy (DR) and glaucoma diseases. Digital retinal image for vessel extraction (DRIVE) database, structured analysis of the retina (STARE) database, high-resolution fundus (HRF) image database, and digital retinal images optic nerve segmentation database (DRIONS-DB) are often used databases to probe the results of DR and glaucoma. Figure 2 presents such publicly available retinal image datasets (Narasimhan et al., 2012; Geetha et al., 2017). Figure 3 shows a typical retinal image and its structure.

Figure 4 Four normal retinal fundus images from STARE dataset, (a) im0035 (b) im0076 (c) im0119 (d) im0236 (see online version for colours)

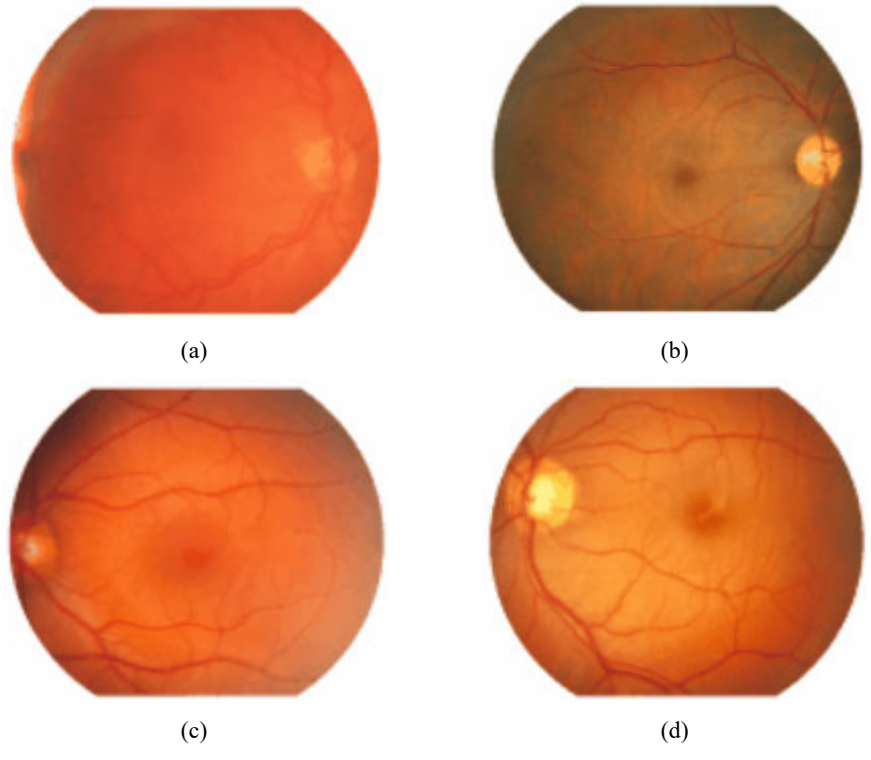

Figure 5 DR (eye disease) (see online version for colours)

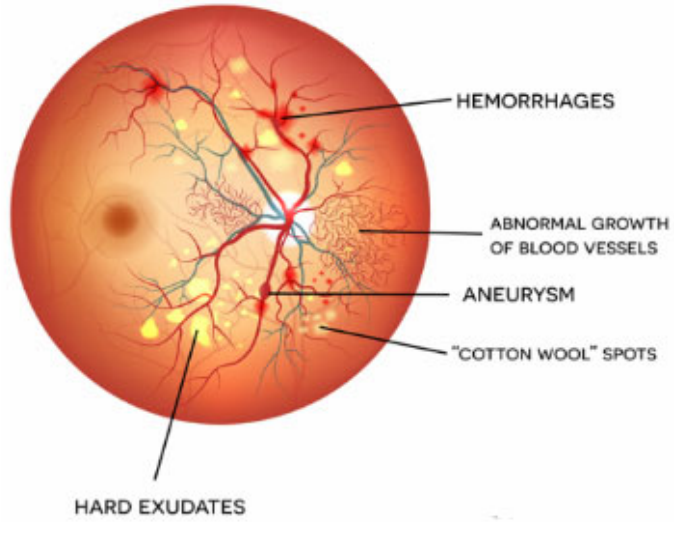

The four normal retinal fundus images (STARE dataset) are shown in Figure 4. It is apparent from the pictures that there are no signs of pathology (disease) like

hemorrhages, aneurysm, hard exudates, abnormal growth of blood vessels and cotton wool spots (Geetha et al., 2017; Stolte and Fang, 2020). Such pathological signs of DR are illustrated in Figure 5. Figure 6 presents the four abnormal retinal images (STARE dataset).

Figure 6 Four abnormal retinal fundus images from STARE dataset, (a) im0113 (b) im0116 (c) im0223 (d) im0247 (see online version for colours)

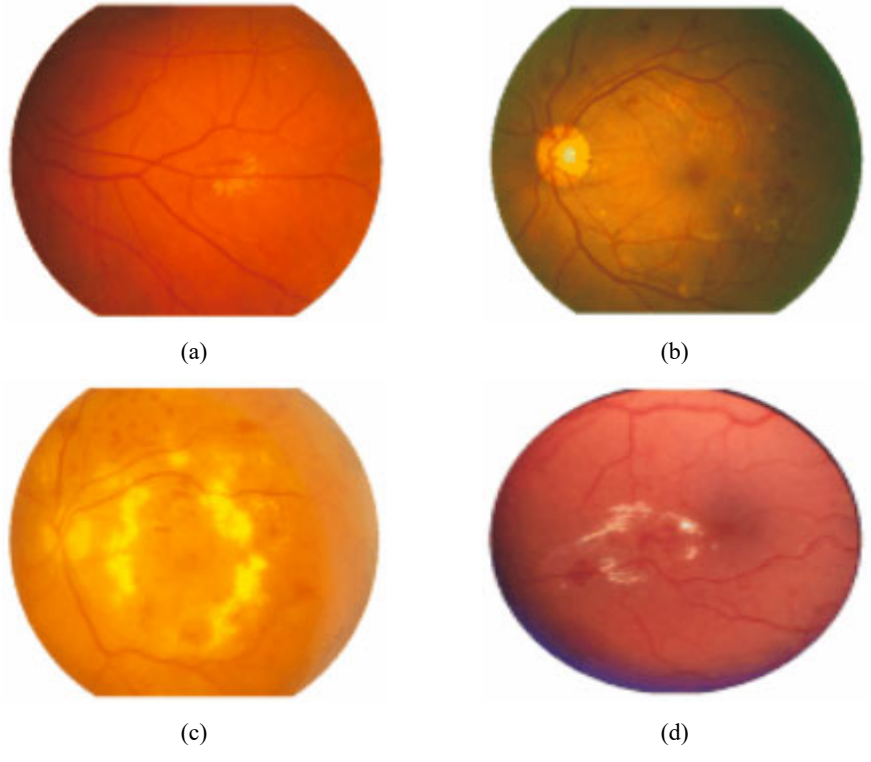

This paper is organised as follows: Section 2 contains the related works (survey) to explore further research in this domain. Section 3 presents the materials and methods, such as image enhancement (pre-processing) tasks on colour retinal fundus images, features extraction, and a classification stages. Simulation results and discussion are described in Section 4. Section 5 contains the conclusions part.

2 Related works

The automatic etection of glaucoma using fundus images often demands to detect and segment the blood vessels. Blood vessel segmentation is a powerful technique since vessels' analysis plays a key parameter not only for diagnosis but also for the clinical treatment and execution. Many methods have been explored for the detection of blood vessel segmentation. The most commonly used techniques (Diaz et al., 2019; Babu and Shenbagadevi, 2011; Kirbas and Quek, 2004) are shown in Figure 7.

Figure 7 Techniques for blood vessel segmentation (see online version for colours)

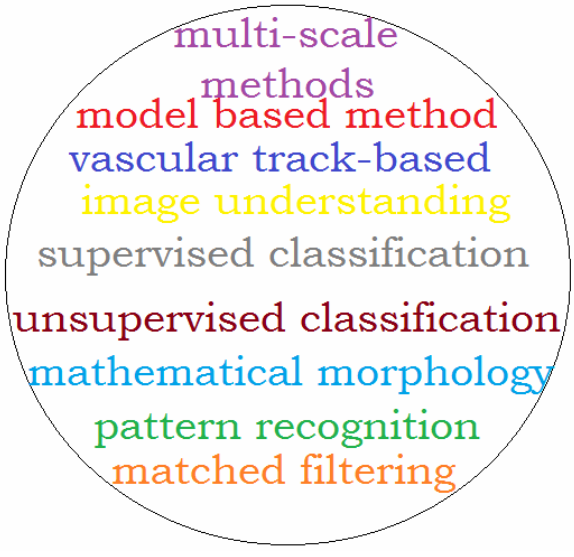

Few researchers demonstrated supervised segmentation techniques using artificial neural networks (NNs) (Zhao et al., 2014; Franklin and Rajan, 2014). Others explored feature extraction, two convolutional neural networks (CNNs), and random forest method to detect blood vessels (Wang et al., 2015). Some researchers, during the training, deployed self-organised maps from the input image and then seen vessels using the k-means algorithm (Lupascu and Tegolo, 2011). In Yin et al. (2013), a probabilistic tracking technique with a Bayesian classifier was explored to identify blood vessels. In Zhang et al. (2014), the authors demonstrated a similar probabilistic approach and a multi-scale line identification method to detect blood vessels.

For the correct blood vessel segmentation, few others explored orthogonal projections of the blood vessel elements texture features (Zhang et al., 2009). The mathematical morphological techniques and k-means algorithm were combined (Hassan et al., 2015) for the blood vessel segmentation. In Abbadi and Saadi (2013), blood vessel segmentation was achieved twofold: one is the advanced image enhancement to remove noise, non-uniform illumination, and low contrast, and the second are with mathematical morphological techniques.

In Singh et al. (2016), the authors used discrete wavelet analysis features from the optic disc (OD). Bit plane analysis was used to locate the OD. Principal component analysis (PCA) and evolutionary parameters were used to detect significant features. A higher accuracy was achieved using a support vector machine for the features generated using PCA. The technique was adopted on a hospital dataset of 63 images with an accuracy of 94%. The classification accuracy can be improved by including clinical features.

Few others (Maheshwari et al., 2017) used a variation mode decomposition method to extract features such as Kapoor, Reyni, Yager and fractal dimension. ReliefF method was used to select the significant features. For training the model, the least square SVM was used to classify a hospital dataset of 488 images. This technique offered a good classification accuracy of 94.79%.

In Noronha et al. (2014), the authors detected higher-order cumulant features from the fundus images. The linear discriminant analysis was used to reduce the extracted feature size. The resultant features were applied to classify normal and glaucoma images using naive Bayes (NB) and SVM classifier. The technique was adopted on a hospital dataset of 272 images. Using the NB classifier, the best accuracy of 92% was obtained. They concluded with a report that accuracy can be improved using clinical features such as a cup-disc ratio (CDR).

In Pathan et al. (2021), the authors explored automated segmentation algorithms for OD and optic cup to overcome the minimised variability present between the region of interest and the background. Also, the segmented regions were used to generate clinical and textural features. The proposed method was applied to a hospital dataset of 300 images and publicly available Drishti dataset.

In Kumar et al. (2016), the authors deployed the blood vessel segmentation process is twofold: one is to apply the contrast limited adaptive histogram equalisation (CLAHE) to the retinal fundus image, and the second is to adopt the Gaussian and Laplacian of Gaussian (LoG) with a binarisation process for the segmentation. Few others demonstrated a matched filter with a Gaussian function of zero-mean to locate blood vessels and computed threshold-based first-order derivative of the resulting image (Zhang et al., 2010).

3 Materials and methods

3.1 Pre-processing

In general, retinal colour fundus images would face critical lighting abnormalities, low contrast and noise. To sort out these difficulties and obtain better images for the diagnosis, image enhancement with pre-processing steps are often required (Marin et al., 2011). The removal of vessel central light reflex, background homogenisation, and vessel enhancement are the crucial steps in the pre-processing, as illustrated in Figure 8.

In the beginning, the green channel is extracted from the retinal colour image since it produces better blood vessel background contrast information. The other two channels, such as red and blue, obtain low contrast and poor dynamic range, respectively (Marin et al., 2011). Naturally, blood vessels look darker than the background because of the minimal reflectance of the retinal parts. Then, the median filter is used to remove the noise components at the early stage. For the better view of the vessel cross-sectional grey level parts, the Gaussian would help but some vessels have a light reflex that flows at blood vessels' middle length. A mathematical morphological opening with a suitable structuring element is used to nullify these brighter chunks. Also, Gaussian and mean filters are used to remove the noise further. To enhance the vessels (segmentation) additionally, the morphological top-hat transformation is adopted. The resulting images during the pre-processing steps are shown in Figure 9. Here, the original image is collected from the STARE dataset.

Figure 8 Pre-processing steps

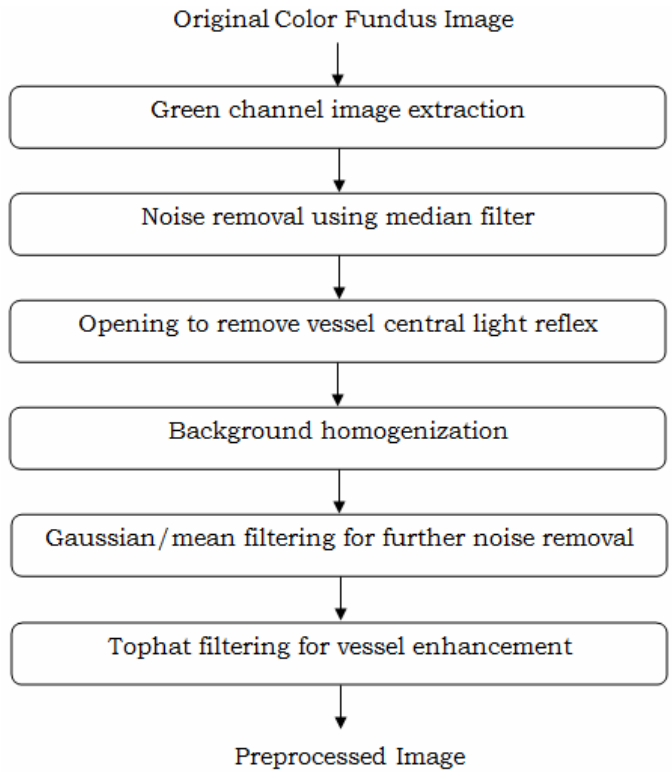

3.2 Features extraction

Image features are useful properties of the image, which play a primary role in image processing. Image features become useful in classifying or detecting images or extracting information from the raw images. This phase is to characterise the pixels in terms of a feature vector with some quantitative measurements that may be useful to categorise them as blood vessels or non-vessels. In this study, the following two sets of features are used for better classification.

Firstly, the grey pixel values of blood vessels are smaller than the surrounding pixel values. Such statistical information is used to extract the features. For example, grey-level features in the fundus image are computed by the difference between grey values in blood vessel pixel and its surrounding pixel's statistical value. As a result, minimum, maximum, mean, and standard deviation become useful statistical measures.

Secondly, the invariant moments are often used effectively in image recognition or classification problems and hence explored as prominent features in various image processing applications (Hu, 1962). These invariant moments never vary because of scaling, rotation and translation of images. Features never change due to scaling, rotation, and translation of images. Hence, invariant moments for every block can be assessed simply with the ground truth image block to identify blood vessels or non-vessel.

Figure 9 Resulting images during the pre-processing step, (a) original retinal colour image (b) extracted green channel (c) median filtered (d) Gaussian and mean filtered (e) the final processed image (see online version for colours)

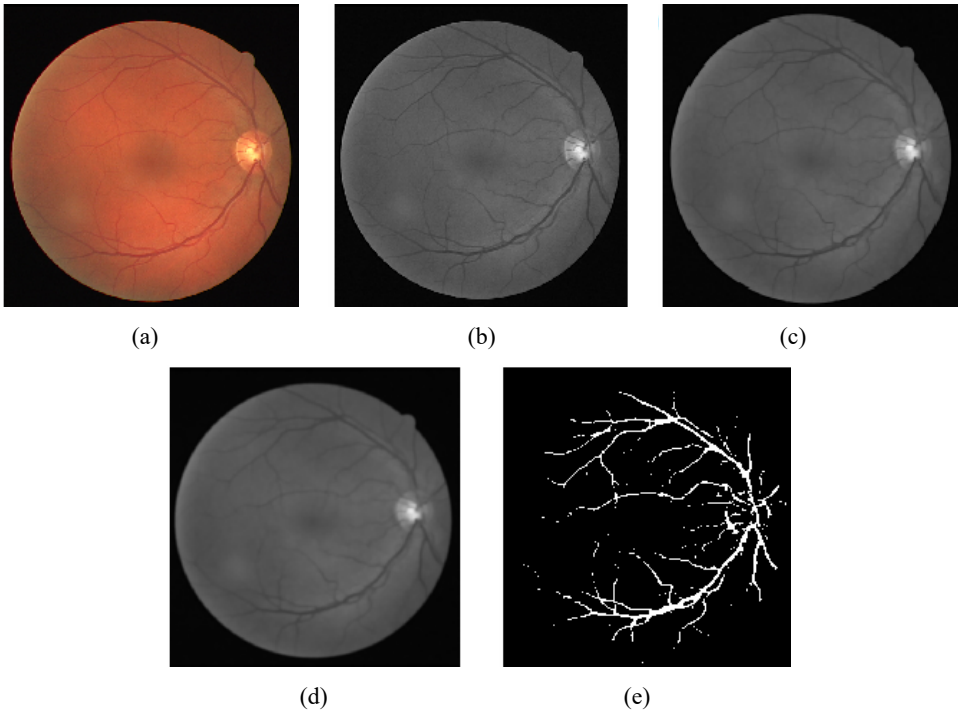

3.3 Classification

The linear classifiers might produce poor results for the separation of blood vessels, and non-vessels and hence the nonlinear classifiers can be used for this study. So any nonlinear classifiers would provide the solution to the blood vessel segmentation problem. The NNs, k-nearest neighbour (k-NN) algorithm, support vector machines, and Bayesian classifiers are the widely used nonlinear classifiers for better classification. A multilayer feed-forward neural network (FFNN) is implemented in this study. To classify the blood vessel or non-vessel pixels, NN classifiers are used in both training and testing phases.

4 Results and discussion

4.1 Dataset used

We experiment with our method on the two publicly available datasets: DRIVE and STARE. The ground truth or manually segmented images by experts supplied in these databases are used to better assess the proposed technique.

4.1.1 DRIVE

The DRIVE dataset contains 40 retinal colour fundus images acquired from a DR screening program organised in the Netherlands (Staal et al., 2004). The images were captured with a Canon CR5 non-mydriatic 3-CCD camera at a 45-degree field of view (FOV). They were stored in 24-bit TIFF with a resolution of 565 × 584 pixels. Three experts' segmentation reports were available. The first expert results were used as ground truth in this study. For the classification model, image27 was used to train the NN, and 20 images (image 01-to-image 20, see Table 1) were used for testing (assessment). For classification tasks, a multiyear FFNN was performed in this study. For training purposes, 20 neurons were used in the hidden layer. The training required more time (20 minutes) than testing (5 seconds only).

Figure 10 A view of NN training (see online version for colours)

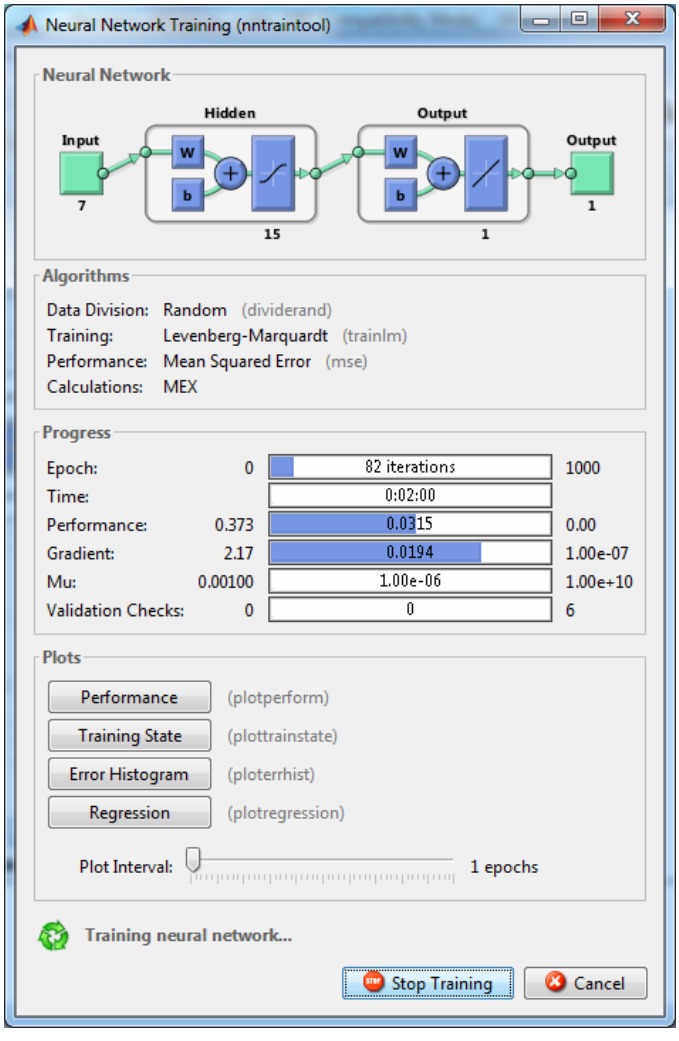

Table 1 Vessel/non-vessel classification

Classification predictions	*Manual identification of a pixel ∈ vessel*	*Manual identification of a pixel ∉ vessel*
Model identifies pixel ∈ vessel	True positive (TP)	False positive (FP)
Model identifies pixel ∉ vessel	False negative (FN)	True negative (TN)

4.1.2 STARE

The STARE dataset includes 20 retinal colour fundus images captured by the TopCon TRV-50 fundus camera at a 35-degree FOV. They were stored in 24-bit TIFF with a resolution of 700 × 605 pixels (Hoover et al., 2000). Among 20 images, 10 images are normal, and the remaining 10 are glaucoma affected images. The two expert segmentation reports were available, but the first one is used here as ground truth for classification purposes. For performance measures, an image77 was used to train the NN model, and the remaining 19 images were used for the testing phase. For classification tasks, a multiyear FFNN was performed in this study. For training purposes, 15 neurons were used in the hidden layer. Again, as expected, the training required more time than the testing. Figure 10 shows a view of the training phase by a NN model.

4.2 Training and testing phases

The frameworks of training and testing evaluation stages are shown in Figures 11 and 12, respectively.

Figure 11 The training phase by a feed-forward backpropagation neural network (FFBN)

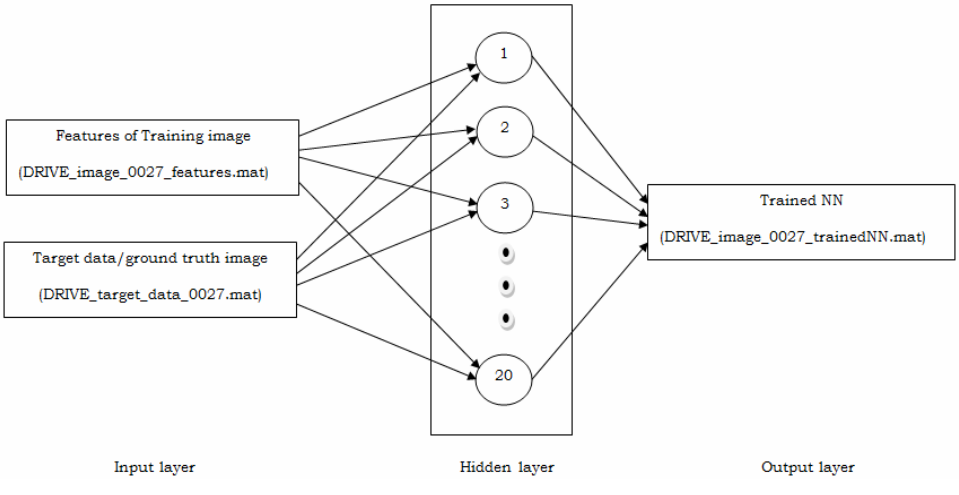

4.3 Classification metrics

Machine learning techniques are useful for clinicians for better diagnosis. In this study, during the blood vessel segmentation process, the event is a pixel-based classification

result. Any pixel might be categorised as a blood vessel or non-vessel. As a result, there are four likelihoods: two classifications and two misclassifications.

Figure 12 The testing phase for the 'test_image_01' using a trained NN

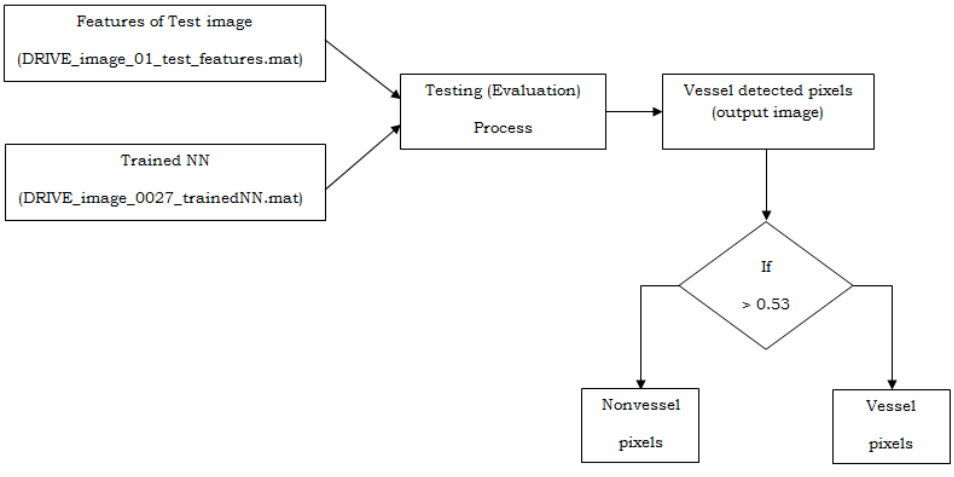

The classifications are the true positive (TP), where a pixel is recognised as the part of the vessel region in both the segmented image and ground truth image, and the true negative (TN) where a pixel is classified as not a part of the vessel region in the segmented image and ground truth image. The two misclassifications are the false negative (FN), where a pixel is marked as non-vessel part in the system processed image but as a vessel part in the ground truth image, and the false positive (FP) where a pixel is sealed as vessel area in the system processed image but to the non-vessel area in the ground truth image. Table 1 summarises the pixel classification.

In this study, the classification procedure was assessed in terms of accuracy (*Acc*), sensitivity (*Se*), specificity (*Sp*), and precision or positive predictive value (*PPV*). Taking Table 1 into account, these metrics are expressed as (Tharwat, 2018)

$$Acc = \frac{TN + TP}{TN + TP + FN + FP} \tag{1}$$

$$Se = \frac{TP}{FN + TP} \tag{2}$$

$$Sp = \frac{TN}{FP + TN} \tag{3}$$

$$PPV = \frac{TP}{FP + TP}. \tag{4}$$

4.4 Simulation results and discussion

Evaluation results in the DRIVE dataset (20 images) and STARE dataset (19 images) are detailed in Tables 2 and 3, respectively. The average accuracies of the DRIVE dataset

and STARE dataset are 93.94% and 95.00%, respectively. Also, the performance comparison results are summarised in Tables 4 (DRIVE) and 5 (STARE). For both the datasets, the average accuracy of this study is computed, compared and tabulated in Tables 4 and 5.

Table 2 Evaluation results in the DRIVE dataset

Image	*Normal (or) DR*	*Acc*	*Se*	*Sp*	*PPV*
01_test.tif	Normal	0.9431	0.6150	0.9752	0.7087
02_test.tif	DR	0.9506	0.7053	0.9785	0.7894
03_test.tif	Normal	0.9375	0.5000	0.9860	0.7977
04_test.tif	DR	0.9570	0.684	0.9846	0.8187
05_test.tif	DR	0.9530	0.6735	0.9818	0.7931
06_test.tif	DR	0.9167	0.2209	0.9917	0.7419
07_test.tif	DR	0.9518	0.6631	0.9809	0.7771
08_test.tif	DR	0.9439	0.5594	0.9801	0.7255
09_test.tif	DR	0.9291	0.2750	0.9867	0.6467
10_test.tif	DR	0.9476	0.5732	0.9812	0.7325
11_test.tif	DR	0.9488	0.6765	0.9755	0.7311
12_test.tif	DR	0.9392	0.4494	0.9855	0.7459
13_test.tif	DR	0.9319	0.4377	0.9855	0.7658
14_test.tif	DR	0.9291	0.3837	0.9771	0.5959
15_test.tif	DR	0.9396	0.6148	0.9647	0.5729
16_test.tif	DR	0.9281	0.3965	0.9809	0.6727
17_test.tif	DR	0.9215	0.1762	0.9902	0.6228
18_test.tif	DR	0.9361	0.3924	0.9829	0.6636
19_test.tif	DR	0.9374	0.4482	0.9816	0.6883
20_test.tif	DR	0.9453	0.5278	0.9784	0.6601

Table 3 Evaluation results in the STARE dataset

Image	*Normal (or) DR*	*Acc*	*Se*	*Sp*	*PPV*
im0001	DR	0.9350	0.3175	0.9885	0.7061
im0002	DR	0.9406	0.4466	0.9758	0.5688
im0003	DR	0.9527	0.6766	0.9703	0.5291
im0004	Normal	0.9430	0.2914	0.9952	0.8280
im0005	DR	0.9156	0.4966	0.9572	0.5356
im0044	DR	0.9460	0.5036	0.9791	0.6437
im0081	Normal	0.9651	0.5823	0.9960	0.9214
im0082	Normal	0.9663	0.7797	0.9822	0.7891
im0139	DR	0.9512	0.5078	0.9900	0.8164
im0162	Normal	0.9626	0.5805	0.9919	0.8463
im0163	Normal	0.9711	0.7466	0.9899	0.8616

Table 3 Evaluation results in the STARE dataset (continued)

Image	*Normal (or) DR*	*Acc*	*Se*	*Sp*	*PPV*
im0235	Normal	0.9562	0.5904	0.9919	0.8774
im0236	Normal	0.9538	0.5494	0.9941	0.9021
im0239	Normal	0.9477	0.6526	0.9756	0.7169
im0240	Normal	0.9263	0.3218	0.9950	0.8804
im0255	Normal	0.9534	0.5454	0.9935	0.8914
im0291	DR	0.9624	0.5295	0.9855	0.6602
im0319	Normal	0.9623	0.4387	0.9859	0.5834
im0324	Normal	0.9378	0.3428	0.9804	0.5554

Table 4 Performance comparisons in the DRIVE dataset

Method	*Accuracy (%)*
Palomera-Perez et al. (2010)	92.5
Ricci and Perfetti (2007)	92.66
Budai et al. (2013)	95.72
Thangaraj et al. (2018)	96.06
Marin et al. (2011)	94.48
Xiao et al. (2013)	95.29
Proposed method	93.94

Table 5 Performance comparisons in the STARE dataset

Method	*Accuracy (%)*
Palomera-Perez et al. (2010)	92.6
Ricci and Perfetti (2007)	94.52
Budai et al. (2013)	93.86
Thangaraj et al. (2018)	94.35
Marin et al. (2011)	94.75
Xiao et al. (2013)	94.76
Proposed method	95.00

5 Conclusions

Our sole objective is to explore the blood vessel segmentation algorithm using a supervised classification approach with an ANN model using grey level and invariant moment feature extraction. Popularly used datasets, such as DRIVE and STARE, are used in this study. Both healthy and DR images are adopted from each dataset for better

results. This study's suggested supervised framework achieved the average vessel segmentation accuracy of 93.94% in the DRIVE dataset and 95.00% in the STARE dataset. This work can be further extended to focus on advanced machine learning techniques such as CNNs and deep learning models for better diagnosis results.

References

Abbadi, N.K.E. and Saadi, E.H.A. (2013) 'Blood vessels extraction using mathematical morphology', *Journal of Computer Science*, Vol. 9, No. 10, pp.1389–1395.

Abramoff, M.D., Garvin, M.K. and Sonka, M. (2010) 'Retinal imaging and image analysis', *IEEE Reviews in Biomedical Engineering*, Vol. 3, pp.169–208.

Babu, T.R.G. and Shenbagadevi, S. (2011) 'Automatic detection glaucoma using fundus image', *European Journal of Scientific Research*, Vol. 59, No. 1, pp.22–32.

Budai, A., Bock, R., Maier, A., Hornegger, J. and Michelson, G. (2013) 'Robust vessel segmentation in fundus images', *International Journal of Biomedical Imaging*, Vol. 2013, No. 154860, pp.1–11.

Diaz, P., Rodriguez, A., Cuevas, E., Valdivia, A., Chavolla, E., Perez-Cisneros, M. and Zaldivar, D. (2019) 'A hybrid method for blood vessel segmentation in images', *Biocybernetics and Biomedical Engineering*, Vol. 39, No. 3, pp.814–824.

Franklin, S.W. and Rajan, S.E. (2014) 'Retinal vessel segmentation employing ANN technique by Gabor and moment invariants-based features', *Applied Soft Computing*, September, Vol. 22, pp.94–100.

Geetha, R., Sugirtharani, S. and Lakshmi, B. (2017) 'Automatic detection of glaucoma in retinal fundus images through image processing and data mining techniques', *International Journal of Computer Applications*, Vol. 166, No. 8, pp.38–43.

Hassan, G., El-Bendary, N., Hassanien, A.E., Fahmy, A., Shoeb, A.M. and Snasel, V. (2015) 'Retinal blood vessel segmentation approach based on mathematical morphology', *Procedia Computer Science*, Vol. 65, No. 2015, pp.612–622.

Hoover, A., Kouznetsova, V. and Goldbaum, M. (2000) 'Locating blood vessels in retinal images by piecewise threshold probing of a matched filter response', *IEEE Transactions on Medical Imaging*, Vol. 19, No. 3, pp.203–210.

Hu, M.K. (1962) 'Visual pattern recognition by moment invariants', *IRE Transactions on Information Theory*, Vol. IT-8, pp.179–187.

Kanski, J.J. and Bowling, B. (2011) *Clinical Ophthalmology: A Systematic Approach*, 7th ed., Elsevier Health Sciences, Edinburgh, New York.

Kirbas, C. and Quek, F. (2004) 'A review of vessel extraction techniques and algorithms', *ACM Computing Surveys*, Vol. 36, No. 2, pp.81–121.

Kumar, D., Pramanik, A.A., Kar, S.S. and Maity, S.P. (2016) 'Retinal blood vessel segmentation using matched filter and Laplacian of Gaussian', in *Proceedings of the IEEE International Conference on Signal Processing and Communications (SPCOM)*, Bangalore, India, pp.1–5.

Kwon, Y.H., Fingert, J.H., Kuehn, M.H. and Alward, W.L. (2009) 'Primary open-angle glaucoma', *New England Journal of Medicine*, Vol. 360, pp.1113–1124.

Lupascu, C.A. and Tegolo, D. (2011) *Automatic Unsupervised Segmentation of Retinal Vessels Using Self-organizing Maps and K-means Clustering*, pp.263–274, Springer, Berlin, Heidelberg.

Maheshwari, S., Pachori, R.B., Kanhangad, V., Bhandary, S.V. and Acharya, U.R. (2017) 'Iterative variational mode decomposition based automated detection of glaucoma using fundus images', *Computers in Biology and Medicine*, 1 September, Vol. 88, pp.142–149.

Marin, D., Aquino, A., Gegundez-Arias, M.E. and Bravo, J.M. (2011) 'A new supervised method for blood vessel segmentation in retinal images by using gray-level and moment invariants-based features', *IEEE Transactions on Medical Imaging*, Vol. 30, No. 1, pp.146–158.

Medha, V. and Pradeep, M. (2014) 'Performance evaluation of optic disc segmentation algorithms in retinal fundus images: an empirical investigation', *International Journal of Advanced Science and Technology*, Vol. 69, No. 2014, pp.19–32, http://dx.doi.org/10.14257/ijast.2014.69.03.

Narasimhan, K., Vijayarekha, K., Narayana, K.A.J., Prasad, P.S. and Kumar, V.S. (2012) 'Glaucoma detection from fundus image using openCV', *Research Journal of Applied Sciences, Engineering and Technology*, Vol. 4, No. 24, pp.5492–5496.

Noronha, K.P., Acharya, U.R., Nayak, K.P., Martis, R.J. and Bhandary, S.V. (2014) 'Automated classification of glaucoma stages using higher order cumulant features', *Biomedical Signal Processing and Control*, Vol. 10, No. 1, pp.174–183.

Palomera-Perez, M.A., Martinez-Perez, M.E., Benitez-Perez, H. and Ortega-Arjona, J.L. (2010) 'Parallel multiscale feature extraction and region growing: application in retinal blood vessel detection', *IEEE Transactions on Information Technology in Biomedicine*, Vol. 14, No. 2, pp.500–506.

Pathan, S., Kumar, P., Pai, R.M. and Bhandary, S.V. (2021) 'Automated segmentation and classification of retinal features for glaucoma diagnosis', *Biomedical Signal Processing and Control*, January, Vol. 63, Article ID: 102244.

Patton, N., Aslam, T.M., MacGillivray, T., Deary, I.J., Dhillon, B., Eikelboom, R.H., Yogesan, K. and Constable, I.J. (2006) 'Retinal image analysis: concepts, applications and potentials', *Progress in Retinal and Eye Research*, Vol. 25, No. 1, pp.99–127.

Ricci, E. and Perfetti, R. (2007) 'Retinal blood vessel segmentation using line operators and support vector classification', *IEEE Transactions on Medical Imaging*, Vol. 26, No. 10, pp.1357–1365.

Sakthivel, K. and Narayanan, R. (2015) 'An automated detection of glaucoma using histogram features', *International Journal of Ophthalmology*, Vol. 8, No. 1, pp.194–200.

Singh, A., Dutta, M.K., Parthasarathi, M., Uher, V. and Burget, R. (2016) 'Image processing based automatic diagnosis of glaucoma using wavelet features of segmented optic disc from fundus image', *Computer Methods and Programs in Biomedicine*, February, Vol. 124, pp.108–120.

Staal, J., Abramoff, M.D., Niemeijer, M., Viergever, M.A. and Van Ginneken, B. (2004) 'Ridge-based vessel segmentation in color images of the retina', *IEEE Transactions on Medical Imaging*, Vol. 23, No. 4, pp.501–509.

Stolte, S. and Fang, R. (2020) 'A survey on medical image analysis in diabetic retinopathy', *Medical Image Analysis*, Vol. 64, No. 101742, pp.1–27.

Thangaraj, S., Periyasamy, V. and Balaji, R. (2018) 'Retinal vessel segmentation using neural network', *IET Image Processing*, Vol. 12, No. 5, pp.669–678.

Tharwat, A. (2018) 'Classification assessment methods', *Applied Computing and Informatics*, 21 August, pp.1–13, in press, DOI: 10.1016/j.aci.2018.08.003.

Wang, S., Yin, Y., Cao, G., Wei, B., Zheng, Y. and Yang, G. (2015) 'Hierarchical retinal blood vessel segmentation based on feature and ensemble learning', *Neurocomputing*, February, Vol. 149, No. PB, pp.708–717.

Xiao, Z., Adel, M. and Bourennane, S. (2013) 'Bayesian method with spatial constraint for retinal vessel segmentation', *Computational and Mathematical Methods in Medicine*, Vol. 2013, No. 401413, pp.1–9.

Yin, Y., Adel, M. and Bourennane, S. (2013) 'Automatic segmentation and measurement of vasculature in retinal fundus images using probabilistic formulation', *Computational and Mathematical Methods in Medicine*, Vol. 2013, No. 260410, pp.1–16.

Zhang, B., Zhang, L., Zhang, L. and Karray, F. (2010) 'Retinal vessel extraction by matched filter with first-order derivative of Gaussian', *Computers in Biology and Medicine*, Vol. 4, No. 4, pp.438–445.

Zhang, J., Li, H., Nie, Q. and Cheng, L. (2014) 'A retinal vessel boundary tracking method based on Bayesian theory and multi-scale line detection', *Computerized Medical Imaging and Graphics*, Vol. 38, No. 6, pp.517–525.

Zhang, Y., Hsu, W. and Lee, M.L. (2009) 'Detection of retinal blood vessels based on nonlinear projections', *Journal of Signal Processing Systems*, Vol. 55, Nos. 1–3, pp.103–112.

Zhao, Y.Q., Wang, X.H., Wang, X.F. and Shih, F.Y. (2014) 'Retinal vessels segmentation based on level set and region growing', *Pattern Recognition*, Vol. 47, No. 7, pp.2437–2446.